Reduction of Unipolar Leakage Flux and Torque Ripple in Consequent-pole PM Vernier Machine

Liang Xu, *Member, IEEE*, Yang Li, Wenxiang Zhao, *Senior Member, IEEE*, and Guohai Liu, *Senior Member, IEEE*

***Abstract*—This paper proposes a new consequent-pole permanent magnet vernier machine (CPMVM), which can be regarded as a combination of two conventional CPMVM with opposite polarities. Based on the simplified axial magnetic circuit model, it is verified that the proposed CPMVM can reduce the unipolar leakage flux. In order to reduce the torque ripple of machine and improve the output torque of machine, the flux barrier is placed on the rotor of the proposed machine. Then, the parameters of the proposed CPMVM are optimized and determined. Moreover, the electromagnetic performance, including no-load air-gap flux density, average torque and torque ripple, flux linkage, back-electromotive force, cogging torque, average torque, torque ripple, power factor and loss, is compared with conventional surface-mounted permanent magnet vernier machine (SPMVM) and CPMVM. Finally, it is demonstrated that proposed CPMVM with flux barrier can effectively reduce the unipolar leakage flux and greatly reduce the torque ripple of machine. Also, compared with the SPMVM, the proposed CPMVM with flux barrier saves more than 45% of the permanent magnet material without reducing output torque.**

***Index Terms*—Consequent-pole, Permanent magnet vernier machine, Unipolar leakage flux, Torque ripple, Flux barrier, Output torque.**

I. INTRODUCTION

DUE to the significant advantages of permanent magnet (PM) machines, such as simple structure, low loss and high power density, experts and scholars at home and abroad have conducted in-depth research on it [1]-[5]. Among many new topologies of PM synchronous machines, permanent magnet vernier machine (PMVM) have entered the field of vision of researchers [6]-[9]. Compared to conventional PM machines, the PMVMs have more sinusoidal no-load back electromotive force (Back-EMF), higher torque density, lower torque ripple. And PMVMs have higher torque densities due to the "magnetic field modulation effect" [10]-[11]. Therefore, PMVM is widely used in low-speed and high-torque occasions [12]-[13].

The premise of PMVM to achieve high torque density and high power density is high magnetic energy rare earth PM. However, as rare earth prices have risen in recent years, cost is one of its main drawbacks. Therefore, many scholars have made efforts to develop PMVM with little or no rare earth PMs [14]-[24]. For example, ferrite PMs are used to replace rare earth PMs in the PM machines [14]-[17]. Also, switched reluctance machine [18]-[20] and hybrid excitation machine [21]-[24] are widely investigated. While reducing the cost of the machines, it also reduces the electromagnetic performance of the machines, such as torque density.

Therefore, for the past few years, more and more experts have proposed a consequent-pole permanent magnet vernier machine (CPMVM) [25]-[29]. In other words, the salient pole core is used to replace the PMs with the same or different polarity of the PM rotor, which can not only save the PM material and improve its utilization rate, but also ensure the higher torque density of the machines. In [25], a novel CP double-rotor PMVM structure was proposed, which not only improves the efficiency and reduces the torque ripple, but also greatly reduces the cost of the machines. A CP, toroidal winding, PMVM had been presented in [26], which reduces the amount of PM while obtaining a higher back-EMF. Therefore, it can be seen that CP PM array is an excellent choice to reduce the cost of machines and has a better application prospect. Although CPMVM has many advantages, but also found its inherent problems. That is, compared with the surface-mounted permanent magnet vernier machine (SPMVM) with N-S pole rotor, the direction of PMs in CPMVM remains the same in radial direction, which leads to the asymmetric of magneto-motive force (MMF) and the unbalance of magnetic field, therefore, the unipolar leakage flux is found in the end shaft, which will reduce the safety and

Manuscript received August 08, 2022; revised November 03, 2022; accepted December 02, 2022. Date of publication March 25, 2023; Date of current version January 17, 2023.

This work was supported in part by the National Natural Science Foundation of China under Projects 52177044 and 52025073, in part by the China Postdoctoral Science Foundation under Project 2019T120395, in part by Hong Kong Scholars Program under Project XJ2019031, in part by the Natural Science Foundation of Jiangsu Higher Education Institutions under Project 21KJA470004, in part by Qing Lan Project of Jiangsu Province, and in part by the Priority Academic Program Development of Jiangsu Higher Education Institutions. *(Corresponding author: Liang Xu.)*

The authors are with the School of Electrical and Information Engineering, Jiangsu University, Zhenjiang, 212013, China, the Jiangsu Key Laboratory of Drive and Intelligent Control for Electric Vehicle, and the National Center for International Research on Structural Health Management of Critical Components, Jiangsu University, Zhenjiang, 212013, China (e-mail: xuliang0511@ujs.edu.cn; 2222007092@stmail.ujs.edu.cn; zwx@ujs.edu.cn; ghliu@ujs.edu.cn).

Digital Object Identifier 10.30941/CESTEMS.2023.00015

reliability of the machine. Although several methods have been mentioned in many literatures to reduce unipolar leakage flux [27]-[29], most of the research targets is conventional PM machines, and the problem of large torque ripple has not been well solved.

Therefore, in this paper, in order to improve the utilization rate of PMs and reduce unipolar leakage flux, a new CPMVM is proposed, which can be equivalent to combining two conventional CPMVM with opposite polarities. In addition, in order to further reduce torque ripple of machine and improve output torque of machines, the flux barriers are embedded into the rotor of the proposed CPMVM.

The paper is organized as follows: In Section II, the machine topologies and the principle of operation of the PMVM is described. Then, based on simplified axial magnetic circuit model, it is verified that the proposed CPMVM can reduce the unipolar leakage flux. The reason for the large torque ripple of the proposed CPMVM is analyzed and the torque ripple is reduced by placing flux barriers on the rotor. In section III, optimizing and determining the machine parameters of the proposed CPMVM. In section IV, compared the electromagnetic properties of all the machines, such as the no-load air-gap flux density, flux linkage, back-EMF, cogging torque, output torque, torque ripple, power factor and loss. The paper is summarized in Section V.

II. PMVM With Different Rotor Structures

A. Machine Topologies

The PMVM with five-phase, 20-slot, 40-flux modulation, and 31-PM pole-pair was used as the research object. Fig. 1(a) shows rotor sequences of all the machines, Fig. 1(b) and (c) shows the conventional SPMVM and CPMVM, i.e, SPMVM and CPMVM1, respectively. Fig. 1(d) shows the proposed CPMVM, namely CPMVM2, which can be equivalent to combining two conventional CPMVM with opposite polarities. In other words, the rotor sequence of the upper part of the machine is arranged in S-iron, while the rotor sequence of the lower part is arranged in N-iron. As can be seen, these machines all use fractional slot concentrated single-layer non-overlapping concentrated winding, with the windings only wound on the armature teeth, which not only reduce the copper in the end windings, but also can isolate the interphase magnetism and heat, thus achieving high fault tolerance. Moreover, it can be seen that each stator tooth has two split teeth, called field modulation poles (FMPs), which are used to modulate the magnetic field generated by the PMs and armature windings. Compared with the structure without FMPs, the advantages of the structure with FMPs are that the concentrated windings can be used to improve the fault tolerance of the machines, and the multi-harmonic design can produce a larger torque density [30]-[32].

B. Principle of Operation

As is known to all, the PMVM operates on the principle of magnetic field modulation effect. FMPs is introduced on the stator teeth of the machine, through which the armature magnetic field with low pole pairs is flux modulated so that it

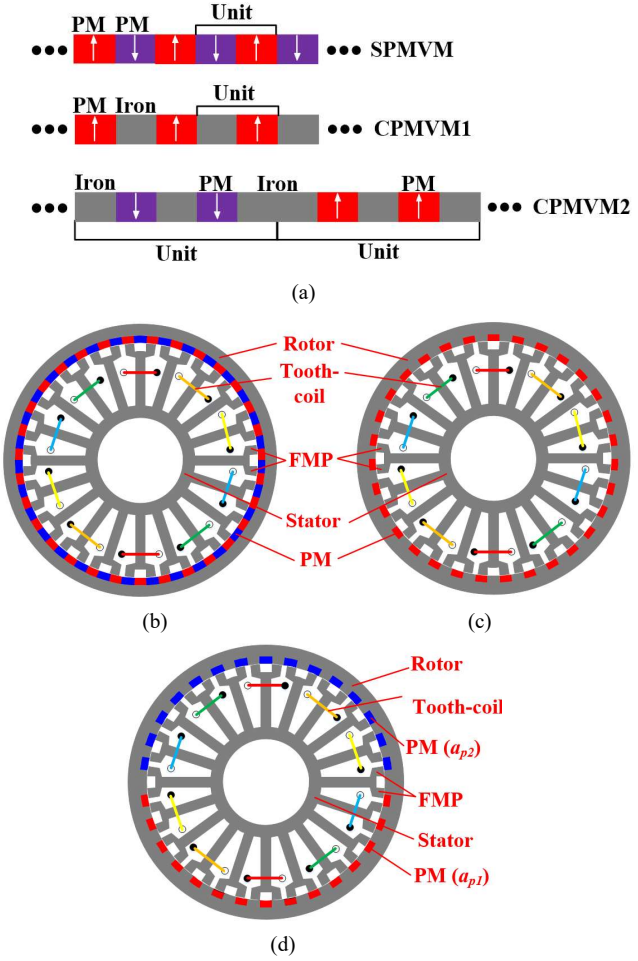

Fig. 1. Topology of 20-slot/62-pole machines with different rotor structures. (a) Rotor sequences. (b) SPMVM. (c) CPMVM1. (d) CPMVM2.

can be matched and interact with the PM field with high pole pairs. In this way, small changes in rotor position can cause significant changes in magnetic field, thus realizing low speed and high torque operation. And the design parameters of the PMVM need to satisfy a certain relationship:

$$Z_s = P_r + P_s \tag{1}$$

where Z_s represents the FMPs number, P_r represents the PM pole-pairs and P_s represents the armature windings pole-pairs. In addition, the armature magnetic field space of the PMVM of each harmonic number of pole-pairs $P_{m,n}$, Z_s, P_s, the angular velocity $\omega_{m,n}$ of the harmonic magnetic field and the angular velocity ω_s of the armature magnetic field should be satisfied as:

$$P_{m,n} = \left| mP_s + nZ_s \right| \tag{2}$$

$$\omega_{m,n} = \frac{mP_s}{mP_s + nZ_s}\omega_s \tag{3}$$

where m=1,3,5…, n=0,±1, ±2, ±3…, when m=1 and n=-1, the stator harmonic rotating magnetic field is the strongest after magnetic field modulation.

C. Elimination of Unipolar Leakage Flux in CPMVM1

Although CP rotor can effectively improve the utilization rate of PMs, the PMs in CPMVM1 only have one excitation direction, which will keep the magnetic fields at the side end

of the machine shaft in one direction, resulting serious unipolar leakage flux occurred in the end shaft of the machine, which will reduce safety and reliability of the machine. F_m represents the PM MMF, R_m represents the PM reluctances, R_g represents the reluctance of the air-gap, R_{end} represents the end air region reluctance.

Fig. 2(a) shows the simplified axial magnetic circuit model of the CPMVM1. Due to the unbalance of the PM MMF, part of the magnetic field lines generated by the end of the PM pass through the end air region and then return to the PM, eventually the axial unipolar leakage flux Φ_1 is generated. Fig. 2(b) shows the simplified axial magnetic circuit of the CPMVM2. Compared with CPMVM1, there are PMs with opposite excitation directions, which improves the unbalance of the PM MMF. Therefore, the flux lines does not pass through the end air region, thus forming the flux Φ_2, which eventually reduces the unipolar leakage flux Φ_1.

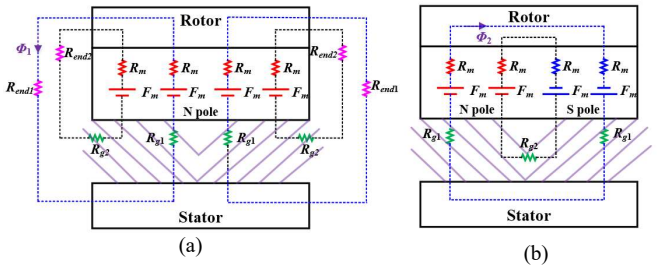

Fig. 2. The simplified axial magnetic circuit models. (a) CPMVM1. (b) CPMVM2.

Fig. 3(a) shows magnetic field distribution on the surface of the end shaft for CPMVM1, and the magnetic field distribution on the surface of the end shaft of CPMVM2 is shown in Fig. 3(b). It can be found that the magnetic field distribution is serious in the CPMVM1, which is up to 0.14T (in average), whereas it is 0.05T (in average) in the CPMVM2. The result is that CPMVM2 can effectively reduce the unipolar leakage flux compared with CPMVM1.

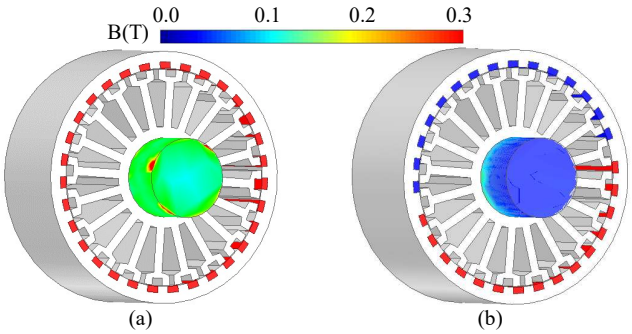

Fig. 3. Magnetic field distribution of the end shaft. (a) CPMVM1. (b) CPMVM2.

D. Reducing Torque Ripple by the Flux Barrier

Although it has been shown in the previous section that the CPMVM2 can effectively reduce unipolar leakage flux, its torque ripple T_{ripple} is found to be large. T_{ripple} and synthetic electromagnetic torque T_e defined as follows:

$$T_{\text{ripple}} = \frac{T_{\max} - T_{\min}}{T_{\text{ave}}} \times 100\% \tag{4}$$

$$T_e = = \sum_{i=A,B,C,D,E} \frac{E_i I_i}{\Omega} \tag{5}$$

where T_{ave} represents the average torque, $T_{\max}$ represents the maximum torque, $T_{\min}$ represents the minimum torque, E represents the effective values of the back-EMF, I represents the effective values of current, Ω represents the mechanical angular velocity.

Taking coil A as an example, Fig. 4 shows the magnetic lines of CPMVM2 under different rotor position in the electric circle. It can be seen that when the PM flux does not pass through the armature teeth, the flux through coil A is zero at this time, as shown in Fig. 4(a). When the rotor of CPMVM2 moves 90°, 180° and 270° respectively, corresponding to Fig. 4(b), (c) and (d), the PM flux passes through the armature teeth, thus the flux through the coil A is not zero. In addition, the flux generated by the PMs of opposite polarity of CPMVM2 directly forms a closed circuit without passing through the air gap, which increases the coupling of CPMVM2. Consequently, the flux waveform of coil A produces large distortion, as shown in Fig. 5(a). And the distortion of the flux caused the sinusoidal degree of the back-EMF of CPMVM2 is not very high, as shown in Fig 5(b). Fig. 6(a) and (b) show variation of each phase electromagnetic torque and synthetic electromagnetic torque waveforms of CPMVM2 with rotor position, respectively. The electromagnetic torque per phase is the theoretical torque that can be achieved by each phase of the machines. From (5), the phase back-EMF is positively correlated with the phase electromagnetic torque. Therefore, the back-EMF has a low sinusoidal degree, which leads to the distortion of electromagnetic torque waveform of each phase, and finally leads to the increase of the torque ripple of CPMVM2.

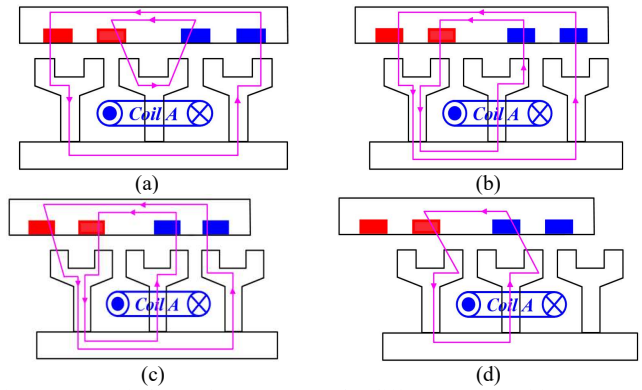

Fig. 4. Magnetic lines of CPMVM2 under different rotor position. (a) 0°. (b) 90°. (c) 180°. (d) 270°.

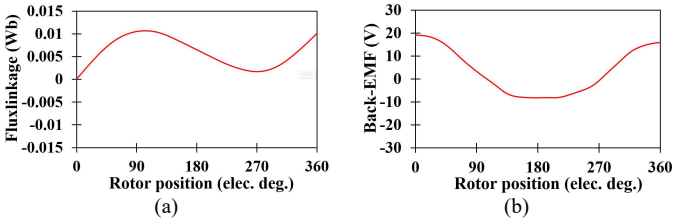

Fig. 5. Coil flux linkage and Back-EMF waveforms of phase A of CPMVM2. (a) Coil flux linkage. (b) Back-EMF.

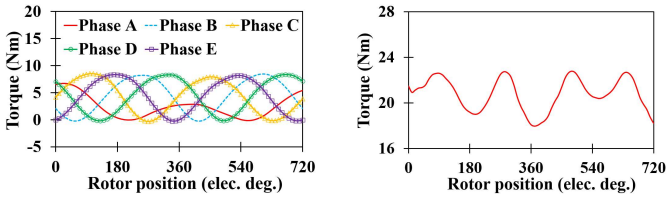

(a) (b)

Fig. 6. Each phase electromagnetic torque and synthetic electromagnetic torque waveforms of CPMVM2. (a) Each phase electromagnetic torque. (b) Synthetic electromagnetic torque.

Therefore, a new rotor structure is proposed to reduce the torque ripple of CPMVM2. Fig. 7 shows the structural transformation of the proposed machines. The key to this design is the placement of flux barriers between two PMs of opposite polarity. The proposed machine with flux barriers is named CPMVM2-1.

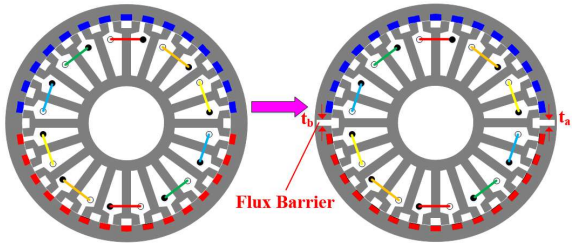

(a) (b)

Fig. 7. Structural transformation of the proposed machines. (a) CPMVM2. (b) CPMVM2-1.

Like CPMVM2, Fig. 8 shows the four characteristic mover positions of CPMVM2-1 in the electric circle. While the difference is when the rotor of CPMVM2-1 runs from 90° to 270°, the flux linkage of coil A changes from positive maximum to negative minimum. What is more, it can be seen that when the flux barrier is embedded into the rotor, the PM flux can pass through the air gap below the iron pole, thus forms two closed circuits, which reducing the coupling of machine. As a result, the distortion of the flux waveform of coil A is improved. As can seen from Fig. 9(b), the sinusoidal degree of the back-EMF of phase A of CPMVM2-1 is increased because of the improvement of the flux waveform. Fig. 10(a) shows each phase electromagnetic torque waveforms of CPMVM2-1, and Fig. 10(b) shows synthetic electromagnetic torque waveforms of CPMVM2-1. Therefore, due to the improvement of back-EMF waveform, the distortion of electromagnetic torque waveform of each phase is improved, which eventually reduces torque ripple.

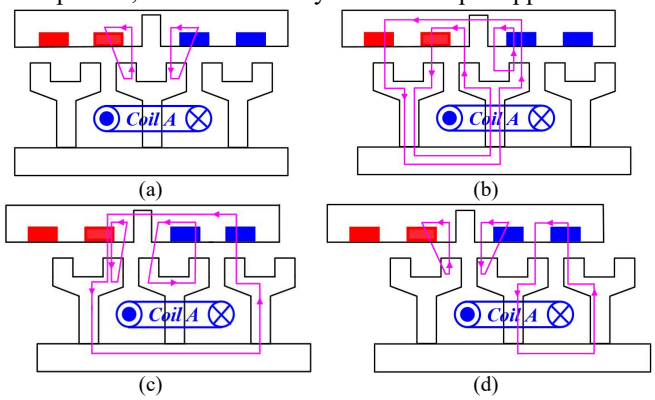

(a) (b) (c) (d)

Fig. 8. Magnetic lines of CPMVM2-1 under different rotor position. (a) 0°. (b) 90°. (c) 180°. (d) 270°.

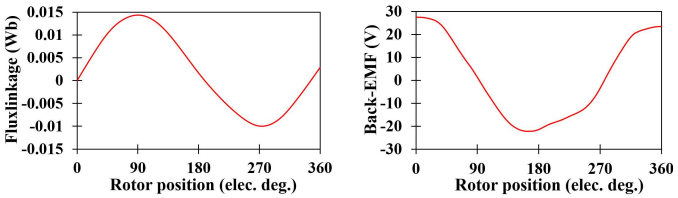

(a) (b)

Fig. 9. Coil flux linkage and Back-EMF waveforms of phase A of CPMVM2-1. (a) Coil flux linkage. (b) Back-EMF.

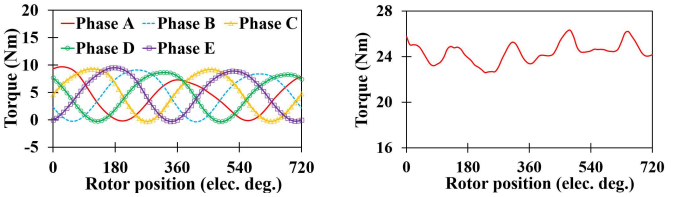

(a) (b)

Fig. 10. Each phase electromagnetic torque and synthetic electromagnetic torque waveforms of CPMVM2-1. (a) Each phase electromagnetic torque. (b) Synthetic electromagnetic torque.

III. Parameter Optimization of the Proposed CPMVM

In the previous section, it was verified that the proposed CPMVM can not only reduce unipolar leakage flux, but also that the CPMVM2-1 can reduce torque ripple. In this section, the parameters of the proposed CPMVM are optimized and determined. And Table I lists the design parameters of all machines.

Before optimizing the machine parameters of the proposed machine, several variables need to be defined. The PM-arc ratio α_p, the ratio of FMPs intertooth slot width to stator slot width k_a and the width ratio of FMPs k_b are defined as:

$$\alpha_p = \frac{\theta_m p_r}{2\pi} \tag{6}$$

$$k_a = \frac{w_a}{w_s} \tag{7}$$

$$k_b = \frac{w_b \times Z_s}{\pi} \tag{8}$$

where θ_m is the PM-arc angles of the CPMVM. Fig. 11 shows parameters of stator teeth, which related to variables k_a and k_b.

TABLE I
DESIGN PARAMETERS OF ALL MACHINES

Parameters	Values
Number of phases	5
PM pole-pair	31
Rotor outside diameter (mm)	70
Rotor inside diameter (mm)	60.5
Stator inside diameter (mm)	22
Air-gap length (mm)	0.5
Axial length (mm)	60
PM thickness (mm)	3.5
Number of coils in series per phase	90
Current density (A/mm^2)	4.87
Rated speed (r/min)	600

A. Optimizing the Flux Barrier Width of the CPMVM2-1

According to the previous analysis, the flux barrier plays a very important role in CPMVM2-1, so the flux barrier width are optimized first. And the width of the two flux barriers of

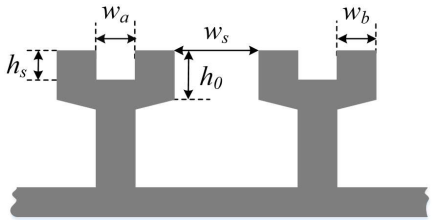

Fig. 11. Parameters of stator teeth.

CPMVM2-1 are defined as t_a and t_b, respectively. Fig. 12(a) show the influence of parameters t_a and t_b on output torque in CPMVM2-1, and the influence of parameters t_a and t_b on torque ripple in CPMVM2-1 is shown in Fig. 12(b). With the increase of t_a and t_b, the output torque also increases, while the torque ripple gradually decreases. Therefore, when the wider the flux barrier width, the better the electromagnetic performance of the CPMVM2-1. However, the width of the flux barrier should not be selected too large, because it will affect the optimization of α_p, thus affecting the electromagnetic performance of the machines. And it can be further found that when t_a and t_b is larger than 3.8mm, the output torque growth of CPMVM2-1 is relatively smooth. Therefore, comprehensive consideration of output torque and torque ripple, t_a=t_b=3.8mm is selected for CPMVM2-1. At this time, both machines have relatively large output torque and relatively small torque ripple.

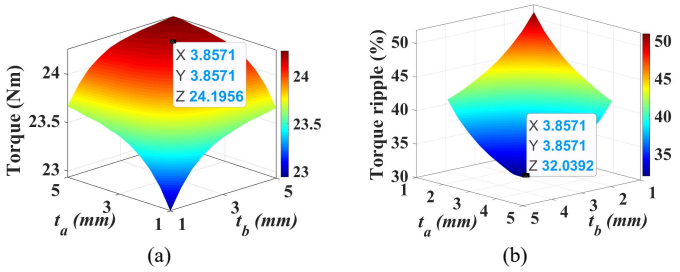

(a) (b)

Fig. 12. Influence of parameters t_a and t_b on output torque and torque ripple in CPMVM2-1. (a) Output torque. (b) Torque ripple.

B. *Optimizing α_p of the Proposed CPMVM*

After the two flux barriers width t_a and t_b of CPMVM2-1 was fixed, the α_{p1} and a_{p2} of the proposed CPMVM was optimized. Fig. 13(a) show the influence of parameters α_{p1} and a_{p2} on output torque and torque ripple in CPMVM2, and the influence of parameters α_{p1} and a_{p2} on output torque and torque ripple in CPMVM2-1 is shown in Fig. 13(b). The output torque and torque ripple of CPMVM2 and CPMVM2-1 have a similar trend with the change of α_{p1} and a_{p2}. It is further found that when the output torque of CPMVM2 and CPMVM2-1 is small, the torque ripple is also small. Because when the α_p is too large, the pole distance of the PMs will become smaller, which will lead to core saturation and affect the performance of the machine. Therefore, when a_{p1}=a_{p2}=0.7 is selected, both CPMVM2 and CPMVM2-1 have relatively large output torque and relatively small torque ripple. Moreover, Compared with CPMVM2, the output torque of CPMVM2-1 is higher, and the torque ripple of CPMVM2-1 is lower.

C. *Optimizing h_s of the Proposed CPMVM*

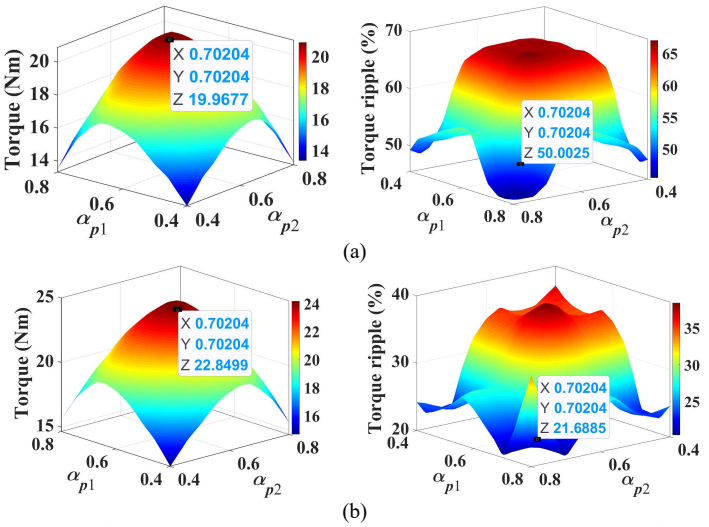

(a) (b)

Fig. 13. Influence of parameters a_{p1} and a_{p2} on output torque and torque ripple in CPMVM2 and CPMVM2-1. (a) CPMVM2. (b) CPMVM2-1.

When the rotor parameters of CPMVM2 and CPMVM2-1 are fixed, Fig. 14(a) and (b) show the influence of FMP height h_s of CPMVM2 and CPMVM2-1 on output torque and torque ripple, respectively. And with the increase of h_s, the output torque of CPMVM2 and CPMVM2-1 both increased first and then decreased, with an obvious regularity. This is because as the height of the FMP increases, the subharmonic amplitude in air-gap flux density will decrease, which increases the output torque. But too high h_s can lead to tooth saturation, resulting in reduced output torque. It can be further found that compared with CPMVM2-1, the torque ripple of CPMVM2 has a more obvious increasing trend, which can be explained by the even harmonics of the back EMFs. This is because that even harmonics of the back EMFs will interact with the current to produce torque ripple. Table II lists the amplitude of even harmonic of phase back EMFs in CPMVM2, while the amplitude of even harmonic of phase back EMFs in CPMVM2-1 are listed in Table III. It can be seen that with the increase of h_s, the increase of the 2nd in CPMVM2-1 is gentle, while for CPMVM2, the increase trend of the 2nd is significantly accelerated from h_s=3mm, as a result, compared with CPMVM2-1, the increase trend of torque ripple of CPMVM2 is significantly larger. It can be found that the output torque of CPMVM2 reaches the maximum value when h_s=1.6mm, while CPMVM2-1 reaches the maximum value when h_s=1.8mm. At this time, the torque ripples of both machines are relatively low. Therefore, h_s=1.6mm is selected for the CPMVM2, and h_s=1.8mm is selected for the CPMVM2-1.

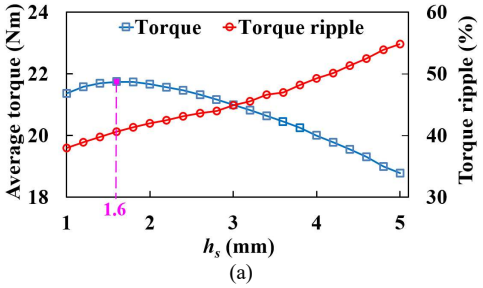

(a)

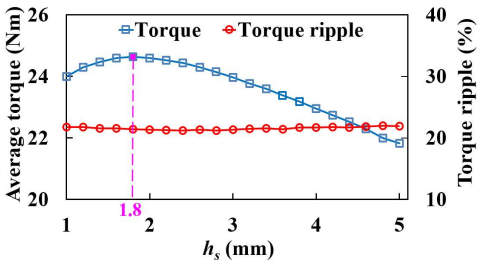

(b)

Fig. 14. Influence of parameters h_s on output torque and torque ripple in CPMVM2 and CPMVM2-1. (a) CPMVM2. (b) CPMVM2-1.

TABLE II
AMPLITUDE OF EVEN HARMONIC OF PHASE BACK EMFS IN CPMVM2

	2nd	4th	6th
h_s=1mm	7.31	3	1.39
h_s=2mm	8.14	3.49	1.32
h_s=3mm	8.49	3.81	1.38
h_s=4mm	9.07	3.86	1.54
h_s=5mm	10.47	3.43	1.41

TABLE III
AMPLITUDE OF EVEN HARMONIC OF PHASE BACK EMFS IN CPMVM2-1

	2nd	4th	6th
h_s=1mm	4.58	0.93	0.34
h_s=2mm	5.28	1.27	0.55
h_s=3mm	5.92	1.48	0.7
h_s=4mm	6.08	1.56	0.72
h_s=5mm	6.24	1.48	0.71

D. *Optimizing k_a and k_b of the Proposed CPMVM*

After fixing the rotor parameters and h_s of CPMVM2 and CPMVM2-1, Fig. 15(a) show the influence of parameters k_a and k_b on output torque and torque ripple in CPMVM2, and the influence of parameters k_a and k_b on output torque and torque ripple in CPMVM2-1 is shown in Fig. 15(b). It can be seen that k_a and k_b affect each other, the change of one variable will lead to the change of the other variable, so these two variables must be optimized at the same time. The output torque and torque ripple of CPMVM2 and CPMVM2-1 have a similar trend with the change of k_a and k_b. That is, with the increase of k_a and k_b, the output torque of the two machines also increases gradually, but the torque ripple is still relatively large on the whole. This is because that k_a and k_b affect the flux distribution in the air gap. Therefore, when k_a=1.6 and k_b=1.1 are selected for CPMVM2, the output torque is relatively large and the torque ripple is relatively small. While for CPMVM2-1, in order to ensure that the output torque is similar to SPMVM and the torque ripple is small, k_a=1.8 and k_b=1 are selected.

Based on the above optimization, Table IV lists the optimized parameter values of the proposed machines and the fixed parameter values of the conventional machines.

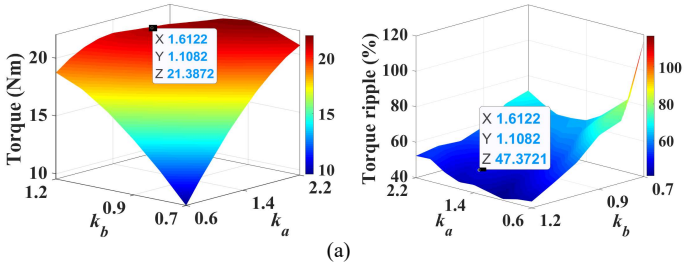

(a)

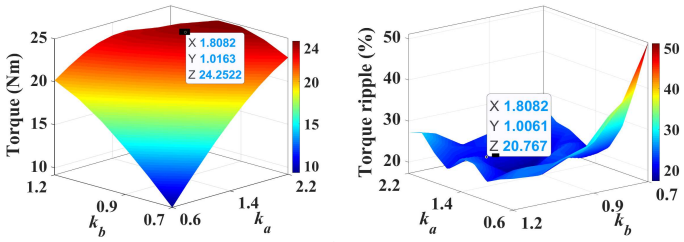

(b)

Fig. 15. Influence of parameters k_a and k_b on output torque and torque ripple in CPMVM2 and CPMVM2-1. (a) CPMVM2. (b) CPMVM2-1.

TABLE IV
OPTIMIZATION PARAMETERS VALUES OF ALL THE MACHINES

Parameters	SPMVM	CPMVM1	CPMVM2	CPMVM2-1
α_{p1}	0.5	0.5	0.7	0.7
α_{p2}	0.5	0.5	0.7	0.7
t_a (mm)	-	-	-	3.8
t_b (mm)	-	-	-	3.8
h_s (mm)	4	4	1.6	1.8
k_a	2.1	2.1	1.6	1.8
k_b	1	1	1.1	1

IV. COMPARISON OF ALL MACHINE PERFORMANCES

Some important parameters of each machine have been determined under the condition of the same current density and rated speed. In this section, the electromagnetic performance of the proposed CPMVM will be analyzed and compared to those of the conventional SPMVM and CPMVM.

A. *No-load Flux Density Distribution*

Fig. 16 shows no-load flux density distribution of all machines, while Fig. 17 (a), (b), (c) and (d) show their no-load airgap flux density waveform and harmonic contents, respectively. It is not difficult to find that the air-gap flux density waveform of all the machines is positive and negative symmetric, as shown in Fig. 17(a) and (b). So all machines only contain odd-order harmonics, and the 31st harmonic is the main working harmonic, as shown in Fig. 17(c) and (d).

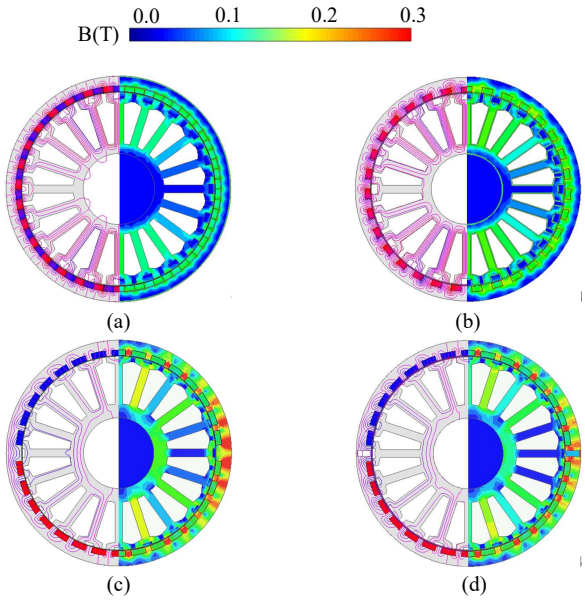

(a) (b) (c) (d)

Fig. 16. Flux density distribution of all machines. (a) SPMVM. (b) CPMVM1. (c) CPMVM2. (d) CPMVM2-1.

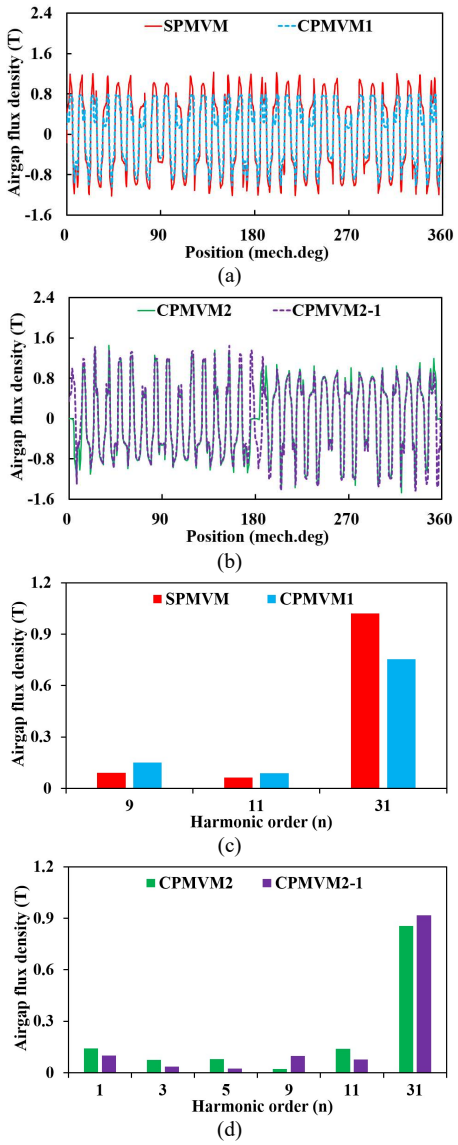

Fig. 17. No-load air-gap flux density of all the machines. (a) Waveforms of conventional machines. (b) Waveforms of proposed machines. (c) Harmonics of conventional machines. (d) Harmonics of proposed machines.

Compared to conventional SPMVM and CPMVM, subharmonics, such as 1st, 3rd, and 5th, appear in the proposed CPMVM. This is because there is a serious coupling phenomenon in CPMVM2 and CPMVM2-1. In other words, the flux generated by the PMs of opposite polarity of CPMVM2 directly forms a closed circuit without passing through the air gap, while the coupling is significantly reduced in CPMVM2-1. Therefore, the subharmonic amplitude of CPMVM2-1 is smaller than that of CPMVM2. In addition, the rotor yoke of the CPMVM2 is highly saturated, which results in the 31st harmonic amplitude of CPMVM2 is low. While in the CPMVM2-1, flux barriers is the adopted to reduce the saturation of rotor yoke, and thus the subharmonics can be suppressed. Therefore, the 31st harmonic amplitude of CPMVM2-1 is larger than CPMVM2. In addition, it can be seen that the 31st harmonic amplitude of the SPMVM is the highest, while the CPMVM1 is the lowest.

B. *Flux Linkage and Back-EMF*

Taking phase A as an example, Fig. 18 shows flux linkage waveforms of all the machines, while Fig. 19 shows back-EMF waveforms of conventional and proposed machines. Compared with the conventional machines, the flux linkage of the CPMVM2 and CPMVM2-1 is distorted, especially CPMVM2. Compared with CPMVM2, the distortion of flux linkage waveform of CPMVM2-1 is greatly improved, so the sinusoidal degree of the back-EMF waveform is improved.

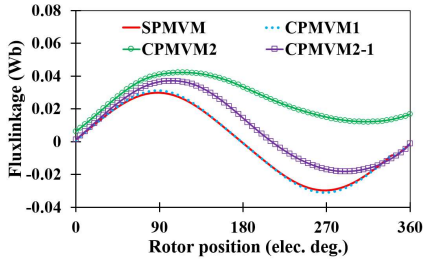

Fig. 18. Flux linkage waveforms of all the machines.

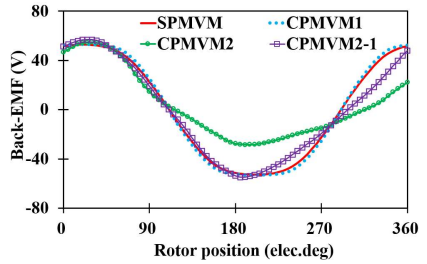

Fig. 19. Back-EMF waveforms of all the machines.

C. *Torque Characteristics*

Fig. 20 shows cogging torque waveforms of all the machines, whilst Table V listes their peak cogging torque T_{cog}. Compared with the conventional machines, the cogging torque of the proposed machines is obviously too large. Moreover, the cogging torque of CPMVM2 is largest among all machines. Compared with CPMVM2, the cogging torque of CPMVM2-1 is reduced.

Fig. 21 shows output torque waveforms of all machines under i_d=0, and Table V lists their torque characteristics, where V_m represents the total PM volume, η_{pm} represents the output torque per total PM volume, and η_{pmu} represents the PM utilization ratio. The output torque of SPMVM and CPMVM2-1 is similar, and the output torque of CPMVM2-1 is lowest among all machines. Moreover, the output torque of CPMVM2-1 is much greater than that of CPMVM2, and compared with CPMVM2-1, the torque ripple of CPMVM2-1 is low. Therefore, the introduction of flux barrier improves output torque and reduces torque ripple, which is consistent with the previous analysis. In addition, compared with SPMVM, the PM utilization ratio η_{pmu} is increased effectively by 30% and 48% for CPMVM2 and CPMVM2-1, respectively.

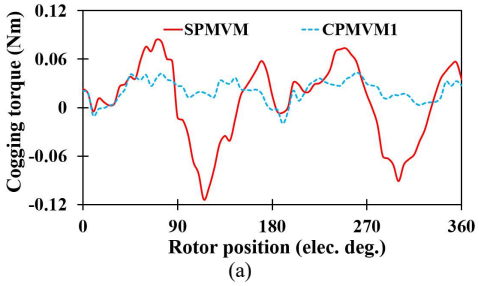

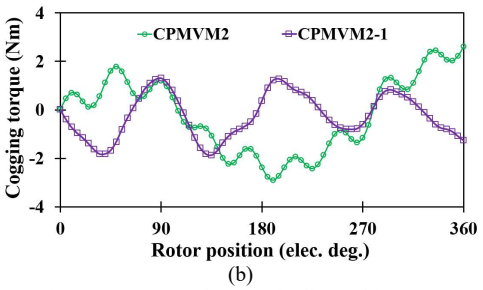

Fig. 20. Cogging torque waveforms of all machines. (a) Conventional machines. (b) Proposed machines.

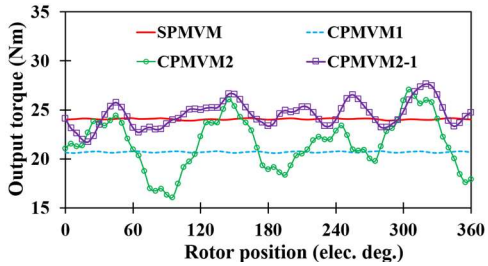

Fig. 21. Output torque waveforms of all machines.

TABLE V
ELECTROMAGNETIC PERFORMANCE OF ALL THE MACHINES

Parameters	SPMVM	CPMVM1	CPMVM2	CPMVM2-1
T_{cog} (Nm)	0.1	0.03	2.75	1.58
T_{ave} (Nm)	24.07	20.69	21.46	24.23
T_{max} (Nm)	24.16	20.79	26	26.71
T_{min} (Nm)	23.92	29.58	16	21.72
T_{ripple} (%)	1	1	46.8	20.6
V_{pm} (mm^3)	4774	2387	3273	3273
η_{pm} (mN/mm^3)	5	8.6	6.5	7.4
η_{pmu} (%)	100	172	130	148

D. Power Factor

Under the control of i_d=0, the power factor can be calculated as:

$$PF = \cos\theta = \frac{1}{\sqrt{1+\left(L_s I_s / \psi_m\right)^2}} \tag{9}$$

where L_s represents the phase winding self-inductance, I_s represents the amplitude of input current, and ψ_m represents the amplitude of PM flux linkage. Table VI lists the I_s, L_s, ψ_m, L_s/ψ_m and the PF of all the machines. The CPMVM1 has the lowest PF in all the machines, since the value of L_s/ψ_m is the largest. And SPMVM and CPMVM2-1 have similar power factor.

TABLE VI
POWER FACTOR OF ALL THE MACHINES

Items	SPMVM	CPMVM1	CPMVM2	CPMVM2-1
I_s (A)	11.21	11.21	12.26	12.19
L_s (mH)	3.3	6.6	4.68	4.4
ψ_m (Wb)	0.03	0.03	0.039	0.037
L_s/ψ_m	110	220	120	118.9
PF	0.66	0.49	0.6	0.65

E. Loss

Fig. 22 shows the distributions of rotor core loss density for the conventional and proposed machines, and Fig. 23 shows the distributions of PM loss density for the conventional and proposed machines. Table VII lists the rotor core loss and the PM eddy loss. The rotor core loss of CPMVM2 is largest among all machines. This is because there is significant coupling in CPMVM2, which leads to saturation of the rotor yoke. While the coupling of the machine is reduced by introducing flux barrier, so the rotor core loss of CPMVM2-1 is lower than that of CPMVM2. The SPMVM has the highest PM eddy loss in all the machines, and the PM eddy loss of CPMVM2 and CPMVM2-1 is similar.

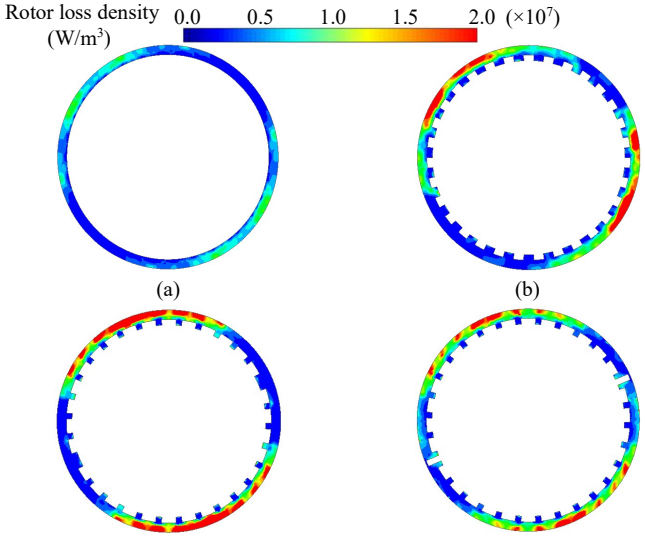

Fig. 22. Rotor loss density under current density of 4.87A/mm^2. (a) SPMVM. (b) CPMVM1. (c) CPMVM2. (d) CPMVM2-1. (600r/min).

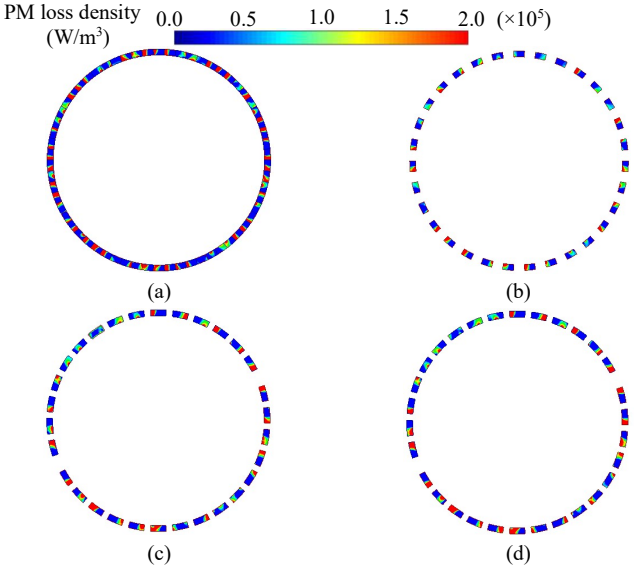

Fig. 23. PM eddy loss density under current density of 4.87A/mm^2. (a) SPMVM. (b) CPMVM1. (c) CPMVM2. (d) CPMVM2-1. (600r/min).

TABLE VII
LOSS OF ALL THE MACHINES

Items	SPMVM	CPMVM1	CPMVM2	CPMVM2-1
Rotor core loss (W)	12.3	38	50	39.9
PM eddy loss (W)	8.36	2.15	6.5	7.05

V. CONCLUSION

In this paper, a new CPMVM is proposed, and the key of this machine is to combine two conventional CPMVM with opposite polarity. Based on simplified axial magnetic circuit model, the principle of reducing unipolar leakage flux is

analyzed. What is more, by placing flux barriers to the rotor of the proposed CPMVM, the distortion of electromagnetic torque waveform of each phase is improved, thus the output torque is increased and the torque ripple is reduced. Then, the parameters of the proposed CPMVM are optimized based on the same current density and speed. The electromagnetic performance of the CPMVM2 and CPMVM2-1, including no-load air-gap flux density, flux linkage, back-EMF, cogging torque, output torque, torque ripple, power factor and loss, is studied and compared with conventional SPMVM and CPMVM. Finally, it is demonstrated that compared with the SPMVM, the proposed CPMVM saves more than 28% of the PM material, and the unipolar leakage flux is reduced. What is more, the CPMVM2-1 can not only reduce torque ripple, but also obtain average torque similar to that of the SPMVM. For the CPMVM2-1, the torque ripple is still large compared with conventional machines, and in the future work, the method of torque ripple reduction will be further studied.

REFERENCES

[1] M. Wang, C. Tong, Z. Song, J. Liu, and P. Zheng, "Performance analysis of an axial magnetic-field-modulated brushless double-rotor machine for hybrid electric vehicles," *IEEE Trans. Ind. Electron.*, vol. 66, no. 1, pp. 806-817, Jan. 2019.

[2] L. Xu, G. Liu, W. Zhao, X. Yang, and R. Cheng, "Hybrid stator design of fault-tolerant permanent-magnet vernier machines for direct-drive applications," *IEEE Trans. Ind. Electron.*, vol. 64, no. 1, pp. 179-190, Jan. 2017.

[3] Z. Xiang, Z. Lu, X. Zhu, M. Jiang, D. Fan, and L. Quan, "Research on magnetic coupling characteristic of a double rotor flux-switching PM machine from the perspective of air-gap harmonic groups," *IEEE Trans. Ind. Electron*., vol. 69, no. 12, pp. 12551-12563, Dec. 2022.

[4] X. Li, Z. Xue, X. Yan, L. Zhang, W. Ma, and W. Hua. "Low-complexity multivector-based model predictive torque control for PMSM with voltage preselection". *IEEE Trans. Power Electron.*, vol. 36, no. 10, pp. 11726-11738, Oct. 2021.

[5] X. Li, Z. Xue, L. Zhang, and W. Hua. "A low-complexity three-vector-based model predictive torque control for SPMSM". *IEEE Trans. Power Electron.*, vol. 36, no. 11, pp. 13002-13012, Nov. 2021.

[6] S. Jiang, G. Liu, W. Zhao, L. Xu, and Q. Chen, "Modeling and analysis of spoke-type permanent magnet vernier machine based on equivalent magnetic network method," *Chin. J. Elect. Eng.*, vol. 4, no. 2, pp. 96-103, Jun. 2018.

[7] W. Zhao, L. Xu, and G. Liu, "Overview of permanent-magnet fault-tolerant machines: Topology and design," *CES Trans. Elect. Mach. Syst.*, vol. 2, no. 1, pp. 51-64, Mar. 2018.

[8] L. Xu, W. Zhao, R. Li, and S. Niu, "Analysis of rotor losses in permanent magnet vernier machines," *IEEE Trans. Ind. Electron.*, vol. 69, no. 2, pp. 1224-1234, Feb. 2022.

[9] L. Xu, W. Wu, and W. Zhao, "Airgap magnetic field harmonic synergetic optimization approach for power factor improvement of PM vernier machines," *IEEE Trans. Ind. Electron.*, vol. 69, no. 12, pp. 12281-12291, Dec. 2022.

[10] M. Cheng, P. Han, and W. Hua, "General airgap field modulation theory for electrical machines," *IEEE Trans. Ind. Electron.*, vol. 64, no. 8, pp. 6063-6074, Aug. 2017.

[11] A. Toba and T. A. Lipo, "Generic torque-maximizing design methodology of surface permanent-magnet vernier machine," *IEEE Trans. Ind. Appl.*, vol. 36, no. 6, pp. 1539-1546, Nov.-Dec. 2000.

[12] Y. Yu, Y. Pei, F. Chai, and M. Doppelbauer, "Analysis of back-EMF harmonics influenced by slot-pole combinations in permanent magnet vernier in-wheel motors," *IEEE Trans. Ind. Electron.*, 2022, doi: 10.1109/TIE.2022.3189065.

[13] D. K. K. Padinharu, G. -J. Li, Z. Q. Zhu, Z. Azar, R. Clark, and A. Thomas, "Effect of airgap length on electromagnetic performance of permanent magnet vernier machines with different power ratings," *IEEE Trans. Ind. Appl.*, vol. 58, no. 2, pp. 1920-1930, March-April 2022.

[14] Q. Chen, S. Eduku, and W. Zhao, "A new fault-tolerant switched flux machine with hybrid permanent magnets," *CES Trans. Elect. Mach. Syst.*, vol. 4, no. 2, pp. 79-86, June 2020.

[15] B. Wang, J. Hu, W. Hua, and Z. Wang, "Fault operation analysis of a triple-redundant three-phase PMA-SynRM for EV application," *IEEE Trans. Transport. Electrific.*, vol. 7, no. 1, pp. 183-192, Mar. 2021.

[16] Z. S. Du and T. A. Lipo, "Design of an improved dual-stator ferrite magnet vernier machine to replace an industrial rare-earth IPM machine," *IEEE Trans. Energy Convers.*, vol. 34, no. 4, pp. 2062-2069, Dec. 2019.

[17] L. Xu, G. Liu, W. Zhao, J. Ji, H. Zhou, and T. Jiang, "Design and analysis of a new linear wound-field flux reversal machine based on magnetic gear effect," *IEEE Trans. Magn.*, vol. 51, no. 11, Nov. 2015, Art. no. 8205004.

[18] X. Li, X. Wang, and S. Yu, "Design and analysis of a novel transverse-flux tubular linear switched reluctance machine for minimizing force ripple," *IEEE Trans. Transport. Electrific.*, vol. 7, no. 2, pp. 741-753, Jun. 2021.

[19] X. D. Xue and N. C. Cheung, "Multi-objective optimization design of in-wheel switched reluctance motors in electric vehicles," *IEEE Trans. Ind. Electron.*, vol. 57, no. 9, pp. 2980–2987, Sep. 2010.

[20] G. J. Li, X. Ma, G. W. Jewell, and Z. Q. Zhu, "Novel modular switched reluctance machines for performance improvement," *IEEE Trans. Energy Convers.*, vol. 33, no. 3, pp. 1255-1265, Sep. 2018.

[21] T. Jiang, W. Zhao, and L. Xu, "Analysis of split-tooth stator PM vernier machines with zero sequence current excitation," *IEEE Trans. Ind. Electron.*, vol. 70, no. 2, pp. 1229-1238, Feb. 2023.

[22] Z. Q. Zhu and S. Cai, "Hybrid excited permanent magnet machines for electric and hybrid electric vehicles," *CES Trans. Elect. Mach. Syst.*, vol. 3, no. 3, pp. 233-247, Sept. 2019.

[23] X. Li, F. Shen, S. Yu, and Z. Xue, "Flux-regulation principle and performance analysis of a novel axial partitioned stator hybrid-excitation flux-switching machine using parallel magnetic circuit," *IEEE Trans. Ind. Electron.*, vol. 68, no. 8, pp. 6560-6573, Aug. 2021.

[24] T. Jiang, W. Zhao, L. Xu, and J. Ji, "A novel parallel hybrid excitation field modulated machine with efficient utilization of multiworking harmonics," *IEEE Trans. Ind. Electron.*, vol. 69, no. 2, pp. 1177-1188, Feb. 2022.

[25] D. Li, R. Qu, J. Li, and W. Xu, "Consequent-Pole toroidal-winding outer-rotor vernier permanent-magnet machines," *IEEE Trans. Ind. Appl.*, vol. 51, no. 6, pp. 4470-4481, Nov.-Dec. 2015.

[26] S. Zheng, X. Zhu, Z. Xiang, L. Xu, L. Zhang, and C. H. T. Lee, "Technology trends, challenges, and opportunities of reduced-rare-earth PM motor for modern electric vehicles," *Green Energy and Intelligent Transportation*, vol. 1, no. 1, 1000012, Jul. 2022.

[27] J. Li, K. Wang, F. Li, S. S. Zhu, and C. Liu, "Elimination of even-order harmonics and unipolar leakage flux in consequent-pole PM machines by employing N-S-iron–S-N-iron rotor," *IEEE Trans. Ind. Electron.*, vol. 66, no. 3, pp. 1736-1747, March 2019.

[28] J. Li, K. Wang, and C. Liu, "Comparative study of consequent-pole and hybrid-pole permanent magnet machines," *IEEE Trans. Energy Convers.*, vol. 34, no. 2, pp. 701-711, June 2019.

[29] K. Wang, J. Li, S. S. Zhu, and C. Liu, "Novel hybrid-pole rotors for consequent-pole PM machines without unipolar leakage flux," *IEEE Trans. Ind. Electron.*, vol. 66, no. 9, pp. 6811-6823, Sept. 2019.

[30] W. Zhao, K. Du and L. Xu, "Design considerations of fault-tolerant permanent magnet vernier machine," *IEEE Trans. Ind. Electron.*, vol. 67, no. 9, pp. 7290-7300, Sept. 2020.

[31] T. Zou, D. Li, R. Qu, D. Jiang and J. Li, "Advanced high torque density PM vernier machine with multiple working harmonics," *IEEE Trans. Ind. Appl.*, vol. 53, no. 6, pp. 5295-5304, Nov./Dec. 2017.

[32] L. Xu, W. Zhao, G. Liu, J. Ji, and S. Niu, "A novel dual-permanent-magnet-excited machine with non-uniformly distributed permanent-magnets and flux modulation poles on the stator," *IEEE Trans. Veh. Technol*., vol. 69, no. 7, pp. 7104-7115, Jul. 2020.

Liang Xu (Member, IEEE) received the B.Sc. degree in electrical engineering and automation from Soochow University, Suzhou, China, in 2011, the M.Sc degree in power electronics and power drives from Jiangsu University, Zhenjiang, China, in 2014, and the Ph.D. degree in control science and engineering from Jiangsu University, Zhenjiang, China, in 2017.

Since 2017, he has been with Jiangsu University, where he is currently an Associate Professor in the School of Electrical Information Engineering. Since 2021, he serves as a Postdoctoral Fellow with the department of Electrical Engineering, The Hong Kong Polytechnic University under Hong Kong Scholars Program. His areas of interest include electrical machines and drives.

Yang Li is currently working towards the M.Sc. degree in electrical engineering from Jiangsu University, Zhenjiang, China. His current research interests include the design and analysis of permanent magnet machines.

Wenxiang Zhao (Senior Member, IEEE) received the B.Sc. and M.Sc. degrees from Jiangsu University, Zhenjiang, China, in 1999 and 2003, respectively, and the Ph.D. degree from Southeast University, Nanjing, China, in 2010, all in electrical engineering.

Since 2003, he has been with Jiangsu University, where he is currently a Professor with the School of Electrical Information Engineering. From 2008 to 2009, he was a Research Assistant with the Department of Electrical and Electronic Engineering, University of Hong Kong, Hong Kong. From 2013 to 2014, he was a Visiting Professor with the Department of Electronic and Electrical Engineering, University of Sheffield, Sheffield, U.K. He is the author or co-author of more than 150 papers published in various IEEE TRANSACTIONS. His current research interests include electric machine design, modeling, fault analysis, and intelligent control.

Guohai Liu (Senior Member, IEEE) received the B.Sc. degree from Jiangsu University, Zhenjiang, China, in 1985, and the M.Sc. and Ph.D. degrees from Southeast University, Nanjing, China, in 1988 and 2002, respectively, in electrical engineering and control engineering.

Since 1988, he has been with the Jiangsu University, where since 2002, he has been a Professor with the School of Electrical Information Engineering. He is currently the Director of Jiangsu Key Laboratory of Drive and Intelligent Control for Electric Vehicle. From 2003 to 2004, he was a Visiting Professor with the Department of Electronic and Electrical Engineering, University of Sheffield, Sheffield, U.K. His teaching and research interests include electrical machines, motor drives for EV and intelligent control. He has authored or co-authored more than 300 technical papers and 4 textbooks, and is the holder of 80 patents in these areas.

Prof. Liu is a Fellow of Institution of Engineering and Technology (IET), UK.